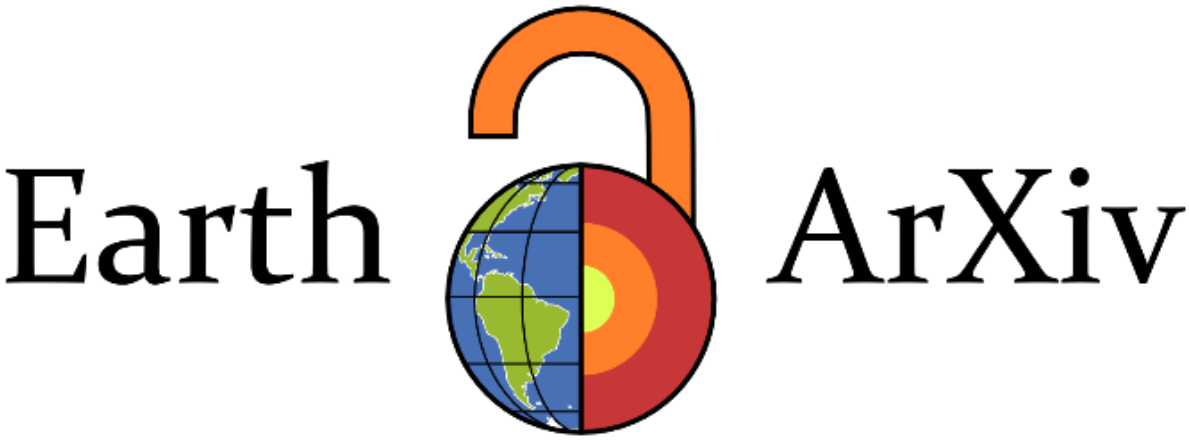

Study on Land-use Change (LUC)-induced carbon emissions

Liaofu Luo [1,*] and Jun Lv [2,*]

[1] Faculty of Physical Science and Technology, Inner Mongolia University, Hohhot 010021, China
[2] College of Science, Inner Mongolia University of Technology, Hohhot 010051, China
*Correspondence
lolfcm@imu.edu.cn (Liaofu Luo); lujun@imut.edu.cn (Jun Lv)
ORCID
0000-0002-6822-185X (Liaofu Luo); 0000-0002-4546-535X (Jun Lv)

Abstract

Land-use change (LUC)-induced carbon emissions (E_{LUC}, defined as net carbon emissions and removals) have accounted for approximately one-third of global anthropogenic carbon emissions since industrialization. While its contribution has declined in recent decades, E_{LUC} still represents a significant component of the global carbon budget, comprising 11% of anthropogenic emissions during 2012–2022. Land-based climate mitigation is essential for meeting the Paris Agreement's climate targets and has attracted growing scientific and political attention in recent years. The complex temporal evolution of E_{LUC} observed both globally and in China highlights land-use change as a key lever for climate mitigation. Investigating E_{LUC} allows for a deeper understanding of climate change dynamics. In this study, we examine a classification framework for complex systems, distinguishing those that are attributable with a dominant driving factor (attributable complex systems with main cause, ACSMC) from those without. The essential dynamics of an ACSMC can be captured via its low-dimensional representations—each time series variable within such a dynamical system can reconstruct these representations. LUC, encompassing deforestation, urbanization, and agriculture across varied regions and territories, collectively forms the optimal fingerprint for the system. Demonstrating the existence of such an optimal fingerprint through simulations of E_{LUC} over time confirms that LUC behaves as an ACSMC. Additionally, we identify three distinct phases in the temporal evolution of E_{LUC}: an increasing phase prior to 1913, a transitional phase from 1913 to 1992, and a declining phase after 1992. Currently in the third phase, we explore the relationships between E_{LUC} and temperature, conduct a detailed statistical analysis, and investigate how land-use change may adapt to future warming.

KeyWords

climate change, carbon emission, (LUC)-induced, attributable complex system, optimal fingerprint, adaption of land-use change

1 Introduction

Land-use change (LUC)-induced carbon emissions (E_{LUC}, defined as the net result of carbon emissions and removals) have accounted for approximately one-third of global anthropogenic carbon emissions since the onset of industrialization. Although their contribution has declined in recent decades, E_{LUC} still constitutes a significant portion of the global carbon budget, representing 11% of anthropogenic emissions during 2012–2022 (Zhu et al. 2025; Friedlingstein et al. 2022). Given the central role of land-based mitigation in achieving the Paris Agreement targets, E_{LUC} has drawn increasing scientific and political attention in recent years (Grassi et al. 2023). In this paper, we compile the temporal evolution of E_{LUC} across different regions and highlight the distinctive characteristics of land-use change-induced carbon emissions.

Two distinct carbon accounting approaches have been used in the literature to characterize E_{LUC} over time (Zhu et al. 2025): the Integrated Biosphere Simulator (IBIS) within the DVGM framework (Foley et al. 1996) and the bookkeeping Land-use Change Emissions (LUCE) model (Qin et al. 2024). The climate system represents a paradigmatic example of a complex system that continuously evolves. Detecting, attributing, and predicting climate change from the perspective of complex system theory has therefore become a critical public concern. Complex system theory has advanced significantly in recent years. Whitney first noted that high-dimensional systems often contain redundant information, and their essential dynamics can be captured through low-dimensional representations (Whitney 1936). Taking inspiration from the detection of strange attractors in turbulence, Takens introduced the delay embedding theorem, which demonstrates that each observable time series variable of a dynamical system can reconstruct a low-dimensional representation and hence produce an isomorphic reconstruction of the full system from a single variable (Takens 1981). Consequently, low-dimensional representations serve as generalized predictors capable of revealing future dynamics in complex systems. More recently, Wu et al. (2024) extended the concept of low-dimensional embedding by integrating feature embedding with delay embedding, thereby broadening the applicability of this framework to real-world systems. Lucarini and Chekroun further demonstrated that response theory for nonequilibrium systems provides the physical and dynamical basis for the optimal fingerprint method, extending it into the nonlinear response regime (Lucarini and Chekroun 2024). Inspired by these developments in complex system theory, we investigate the dynamics of E_{LUC} in this paper.

In recent years, complex adaptive systems (CAS) have attracted considerable attention. These systems are characterized by the interactions among large numbers of adaptive agents, and it is precisely this adaptability that generates the observed complexity (Holland 1992). Within this context, we explore the potential for thermal adaptation of LUC. By deriving the relationship between E_{LUC} and temperature, we analyze E_{LUC} as a function of temperature — denoted $E_{LUC}(T)$ — and assess the

possibility that E_{LUC} may adapt to future warming. Such adaptation would imply a weaker positive carbon–climate feedback in response to rising temperatures.

2 Materials and Methods

2.1 Carbon emissions data

Carbon emissions data are sourced from the supplementary materials of the Global Carbon Budget (GCB) 2025 (Version 1.0) [Data set] (https://doi.org/10.18160/gcp-2025; accessed 10 November 2025), which include both fossil fuel emissions and land-use change emissions (Friedlingstein et al. 2025). The fossil fuel emissions data provide national-level estimates that comprise emissions from fossil fuel combustion, oxidation, and cement production but exclude emissions from bunker fuels; however, global totals do include bunker fuel emissions.

The land-use change emissions component relies on E_{LUC} estimates derived from three models: LUCE (Qin et al. 2024), BLUE (Hansis et al. 2015), and OSCAR (Gasser et al. 2020). The GCB reported E_{LUC} values correspond to the ensemble mean of these three model simulations.

2.2 Global surface temperature anomaly data

Global annual and monthly mean surface temperature anomalies (land and ocean combined) from 1880 to 2025, referenced to the 1880–1920 baseline, are obtained from NASA/GISS/GISTEMP v4 (GISTEMP Team, 2025: GISS Surface Temperature Analysis (GISTEMP), version 4. NASA Goddard Institute for Space Studies. Dataset accessed 2025-12-27 at https://data.giss.nasa.gov/gistemp/; Lenssen et al. 2024). The monthly anomalies were smoothed using locally weighted scatterplot smoothing (LOWESS; Cleveland 1979) with a one-year window, yielding a degree of smoothing comparable to that of a one-year running mean.

To characterize the temperature dependence more precisely, we examined the episodic peak structures in the annual global mean temperature (AGMT) anomalies from January 1880 to November 2025. The series exhibits six discernible peaks between 1929.5 and 1950.7, followed by eighteen peaks from 1950.8 to 2021.3. For the latter eighteen peaks, occurring between 1950 and 2021, we summarize the mean E_{LUC} and corresponding AGMT values for each interval in Table 1.

3 Results

3.1 The uniqueness of Land-use change (LUC)-induced carbon emissions (E_{LUC})

Fig. 1 compares the temporal evolution of fossil carbon emissions for the world and China from 1880 to 2024. Both trajectories exhibit a monotonically increasing trend. In contrast, Figs. 2a and 2b present the net carbon emissions from land-use change for the world and China, respectively, over the same period. These E_{LUC} trajectories are far from monotonic: particularly after 1950, both global and Chinese E_{LUC} have undergone substantial changes and dramatic fluctuations whose amplitudes are comparable to their mean values. Land-use change encompasses deforestation, urbanization, agriculture, and their

combined effects across different regions and territories. These results demonstrate that E_{LUC} is a component of the global carbon cycle that is highly sensitive to anthropogenic activities (Friedlingstein et al. 2022), making it a valuable handle for examining the complex problem of climate change.

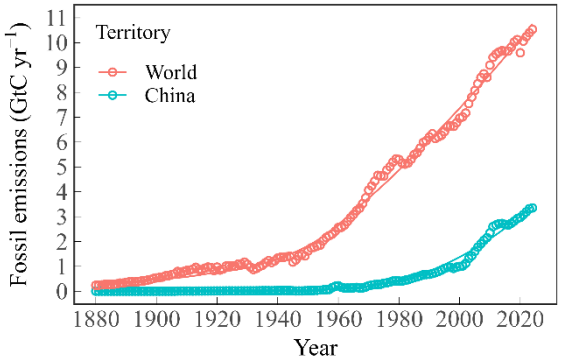

Fig. 1 Fossil carbon emissions by territory. Data are from Friedlingstein et al. (2025). National-level estimates include emissions from fossil fuel combustion, oxidation, and cement production, but exclude international bunker fuels; global totals incorporate all territorial emissions as well as bunker fuel emissions. Solid lines represent LOESS-smoothed curves designed to guide the eye

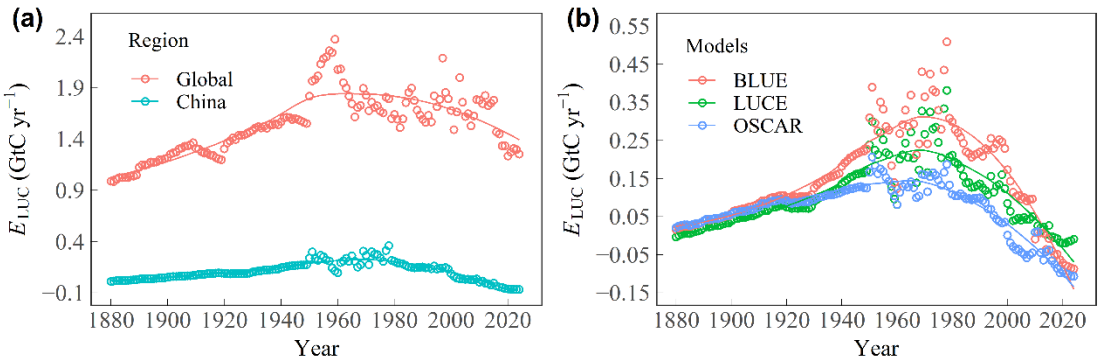

Fig. 2 (**a**) Comparison of net carbon emissions from land-use change between China and the global context. Data are from Friedlingstein et al. (2025). Both the Chinese and global estimates represent the ensemble mean of the three bookkeeping models BLUE, OSCAR, and LUCE. (**b**) Net carbon emissions induced by land-use change within China during 1880–2024 as estimated by the three bookkeeping models. Solid lines depict LOESS-smoothed curves that emphasize the overall trends

3.2 The law of E_{LUC} changing with time

The climate system exemplifies a complex system that evolves over time. E_{LUC} can be regarded as an attributable complex system with a dominant driver, and hence we assume that its essential dynamics can be captured through suitable low-dimensional representations. Following Takens (1981), individual variables from a time series can be employed to reconstruct such representations, providing insight into the underlying dynamics. Figs. 3a and 3b present the evolution of E_{LUC} in China from 1880 to 2024 based on the GCB ensemble simulation and the LUCE model simulation, respectively.

In the GCB simulation, the E_{LUC} time series can be well approximated by a piecewise model comprising three distinct segments. The first segment (1880–1913) exhibits a linear trend with a

positive slope (R^2 = 0.99). The second segment (1913–1992) is best captured by a Gaussian peak function (R^2 = 0.64), while the third segment (1992–2024) returns to a linear trend but with a negative slope (R^2 = 0.94). The LUCE-based simulation yields analogous results, with corresponding R^2 values of 0.99, 0.63, and 0.85 for the three segments. These three phases respectively reflect an increasing phase prior to 1913, a peaked (Gaussian-like) phase between 1913 and 1992, and a declining phase after 1992.

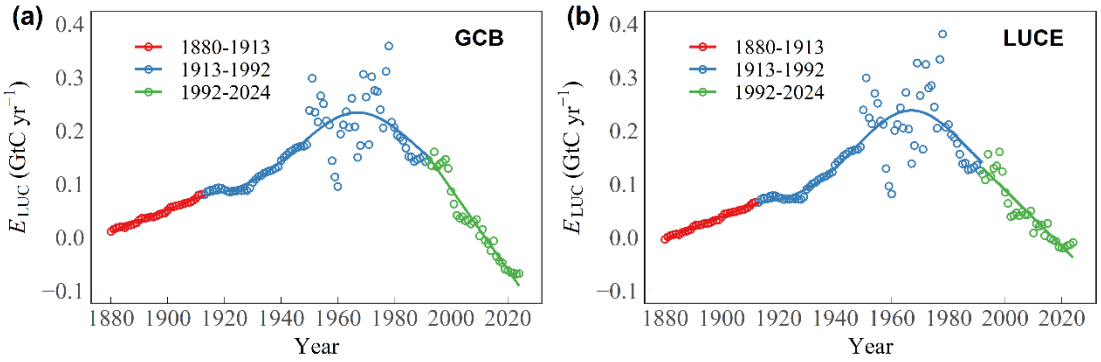

Fig. 3 Temporal evolution and segmented fitting of E_{LUC} in China from 1880 to 2024. (**a**) Estimates are based on the GCB, representing the ensemble mean of three bookkeeping models. The optimal fit is composed of three segments: 1880–1913 (linear fit), 1913–1992 (Gaussian fit), and 1992–2024 (linear fit), with corresponding R^2 values of 0.99, 0.64, and 0.94. (**b**) Estimates are derived from the LUCE model (Qin et al. 2024) as incorporated in the Global Carbon Budget 2025. The same three intervals yield R^2 values of 0.99, 0.63, and 0.85, respectively

Notice: The comparison of net carbon emissions from land-use change between China and the global context (Fig. 2a) highlights the similarity in E_{LUC} evolution across different territories worldwide.

Our findings can be compared with earlier simulations reported in the literature. Zhu et al. (2025) employed two carbon accounting approaches over the period 1981–2020: the Integrated Biosphere Simulator (IBIS) within the DVGM framework and the bookkeeping Land-use Change Emissions (LUCE) model. Fig. 4 presents the IBIS and LUCE simulations of E_{LUC} for this interval, facilitating a direct comparison with our results.

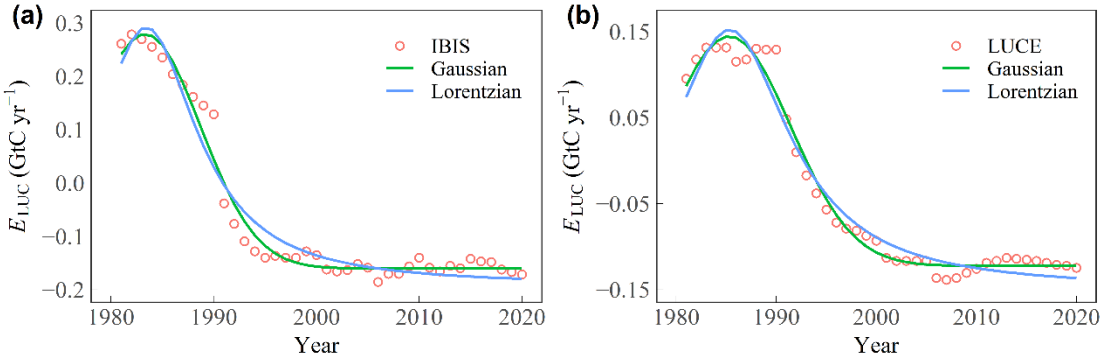

Fig. 4 Simulations of land-use change-induced carbon emissions (E_{LUC}) in China for 1981–2020 based on the IBIS and LUCE datasets. Data are adapted from Fig. 1 of Zhu et al. (2025); the original source does not provide data for 1880–1980. (**a**) E_{LUC} analysis derived from the IBIS model. Gaussian and Lorentzian fits yield R^2 values of 0.98

and 0.96, respectively. (**b**) E_{LUC} analysis derived from the LUCE model. Gaussian and Lorentzian fits yield R^2 values of 0.98 and 0.97, respectively

3.3 Temperature dependence of E_{LUC}

Fig. 5 illustrates the relationship between China's land-use change-induced carbon emissions (E_{LUC}) from 1880 to 2024 and the global annual mean temperature (AGMT) anomalies referenced to the 1880–1920 pre-industrial baseline. By combining the temporal evolution shown in Fig. 3 with the temperature dependence in Fig. 5, we gain insight into how E_{LUC} varies both with time and with AGMT. For example, the current third phase of E_{LUC} evolution corresponds to a regime in which E_{LUC} decreases as AGMT increases, observable along the right-hand side of the four panels in Fig. 5. Notably, the generalization of E_{LUC}–AGMT relationships across regions beyond China remains an open topic for future research.

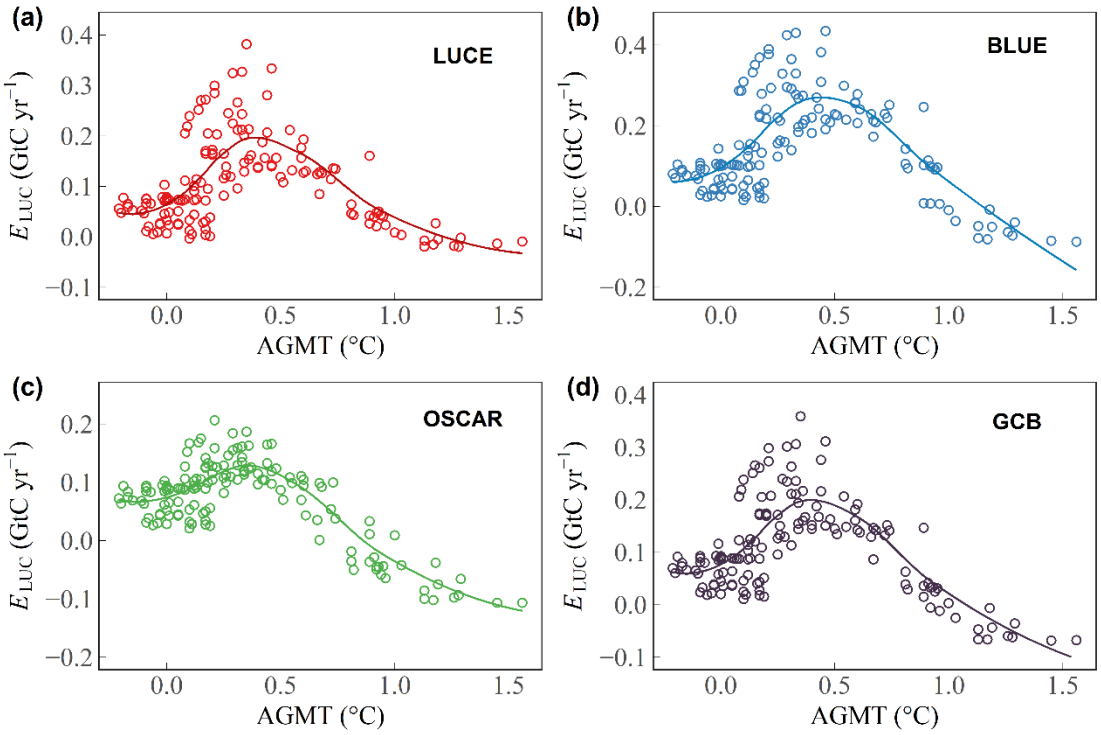

Fig. 5 Relationship between land-use change-induced carbon emissions (E_{LUC}) in China (1880–2024) and annual global mean temperature (AGMT) anomalies relative to the 1880–1920 pre-industrial baseline. Panels (**a**), (**b**), and (**c**) present E_{LUC} estimations from the LUCE, BLUE, and OSCAR bookkeeping models, respectively. Panel (**d**) shows the GCB estimate, representing the multi-model mean of the three bookkeeping models. Solid lines represent LOESS-smoothed curves to emphasize the underlying trends

3.4 E_{LUC} statistical distribution changes with temperature

Fig. 5 shows that a given AGMT can correspond to multiple E_{LUC} values, indicating a probabilistic relationship between temperature and land-use change emissions. We denote the most probable E_{LUC} value at each AGMT by $E'(T)$, as depicted in Fig. 6a. For any infinitesimal increase dT, the temperature sensitivity of E_{LUC}, $\Delta E_{LUC}(T)$, is defined by d^2E'/dT^2 (>0) on the position of dE'/dT =0. The distribution

of ΔE_{LUC} (T) (for dT = 0.001 °C) is given in Fig. 6b.

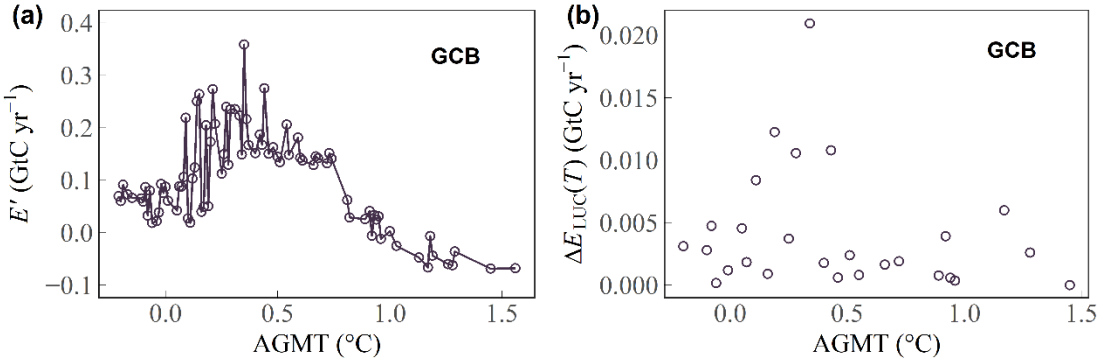

Fig. 6 (**a**) The most probable E_{LUC} value (E') as a function of AGMT. (**b**) Distribution of $\Delta E_{\mathrm{LUC}}(T)$ versus AGMT

3.5 Adaption of land-use change

We characterize the temperature response of E_{LUC} through a Taylor expansion around a reference temperature T_0:

$$E_{\mathrm{LUC}}(T) = E_{\mathrm{LUC}}(T_0)[1 + b(T - T_0) + \cdots], \quad b = \frac{1}{E_{\mathrm{LUC}}(T_0)} \frac{\mathrm{d}E_{\mathrm{LUC}}}{\mathrm{d}T}\Big|_{T=T_0}, \tag{1}$$

where T is expressed in °C, $E_{\mathrm{LUC}}(T_0)$ represents the baseline emission rate at T_0, and b captures the normalized sensitivity of E_{LUC} to temperature in the linear approximation. Thus, $E_{\mathrm{LUC}}(T_0)$ and $bE_{\mathrm{LUC}}(T_0)$ correspond to the intercept and slope of the linearized temperature response, respectively.

From Section 3.3, we observe that E_{LUC} decreases with AGMT in the regime AGMT > 0.4 °C, with the negative trend stabilizing beyond AGMT > 0.9 °C. This indicates that a negative correlation between E_{LUC} and the AGMT gradient emerges only at higher temperatures when fitted by linear regression. The proportional response of E_{LUC} to a small temperature increment (dT = 0.001 °C), denoted $\Delta E_{\mathrm{LUC}}(T)$, defines the temperature sensitivity parameter. Fig. 6b reveals that although the dependence of $\Delta E_{\mathrm{LUC}}(T)$ on AGMT is complex, it increases for AGMT > 0.5 °C. We quantify this trend by regressing $\Delta E_{\mathrm{LUC}}(T)$ against AGMT:

$$\Delta E_{\mathrm{LUC}}(T) = a_1 \times \mathrm{AGMT}, \tag{2}$$

where a_1 is positive for T > 0.5 °C.

Similarly, we evaluate the baseline emissions' dependence on AGMT via

$$E_{\mathrm{LUC}}(T_0) = a_2 \times \mathrm{AGMT}, \tag{3}$$

with a_2 taking negative values for T_0 > 0.4 °C.

In summary, during the third phase of E_{LUC} evolution, the emissions E_{LUC} decrease with temperature while the sensitivity parameter ΔE_{LUC} (T) increases for T > 0.5 °C. The opposing signs of a_2 and a_1 imply that although warming initially raises E_{LUC}, this increase weakens as temperatures rise further, potentially reverting toward pre-warming levels at an accelerated rate. Such stronger thermal adaptation corresponds to a weakening of the positive carbon–climate feedback.

4 Discussions and Summary

4.1 Statistical investigation of the E_{LUC}–temperature relationship

Our analysis reveals that E_{LUC} decreases steadily with global mean surface temperature anomalies (relative to the 1880–1920 baseline) once AGMT surpasses ~0.9 °C (Fig. 5). This pattern suggests that E_{LUC} begins to exhibit adaptive behavior only at relatively high levels of global warming. However, owing to the considerable uncertainty in annual global temperature anomalies—stemming from a multitude of climatic and non-climatic factors—further detailed statistical characterization of this relationship is warranted.

To probe the E_{LUC}–AGMT linkage in greater granularity, we focus on the temperature anomaly peaks occurring between 1950.8 and 2021.3. As illustrated in the right-hand portion of Fig. 7, eighteen such peaks are identifiable within this interval.

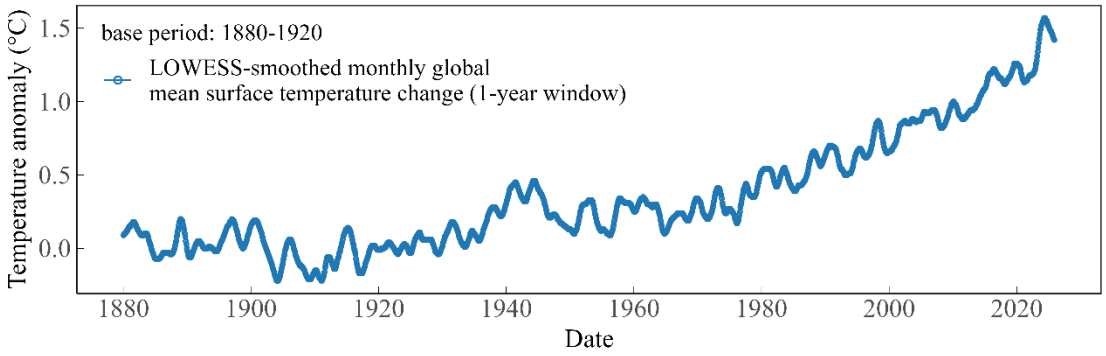

Fig. 7 Monthly averaged temperature anomaly (1-year LOWESS smoothing) from January 1880 to November 2025. Six peaks are evident between 1929.5 and 1950.7, followed by eighteen peaks between 1950.8 and 2021.3

Given the large post-1950 fluctuations in E_{LUC} shown in Figs. 2 and 3, we examine these eighteen peaks and report their corresponding averaged E_{LUC} values and AGMT anomalies in Table 1.

Table 1 Averaged E_{LUC} values for each of the 18 temperature peaks (1950–2021) and the corresponding global temperature anomalies

Peak	Period (Y.M-Y.M)	AGMT(°C)	E_{LUC} (GtC yr^{-1}) (China)			
			LUCE	BLUE	OSCAR	GCB
1	1950.08-1956.03	0.11 (+0.11)	0.25	0.32	0.17	0.25
2	1956.04-1960.02	0.12 (+0.11)	0.15	0.20	0.12	0.16
3	1960.03-1964.10	0.26 (+0.05)	0.19	0.26	0.12	0.19
4	1964.11-1968.06	0.10 (+0.07)	0.20	0.28	0.12	0.20
5	1968.07-1971.07	0.18 (+0.08)	0.23	0.32	0.13	0.23
6	1971.08-1974.05	0.15 (+0.13)	0.26	0.36	0.15	0.26
7	1974.06-1976.02	0.24 (+0.02)	0.24	0.33	0.15	0.24
8	1976.03-1978.09	0.17 (+0.13)	0.31	0.41	0.16	0.29
9	1978.10-1982.05	0.33 (+0.10)	0.24	0.33	0.13	0.23
10	1982.06-1985.03	0.43 (+0.06)	0.16	0.25	0.10	0.17
11	1985.04-1989.03	0.35 (+0.16)	0.13	0.21	0.10	0.15
12	1989.04-1993.03	0.55 (+0.07)	0.12	0.22	0.09	0.14
13	1993.04-1996.05	0.45 (+0.11)	0.13	0.24	0.06	0.14
14	1996.06-1999.09	0.55 (+0.16)	0.14	0.24	0.04	0.14
15	1999.10-2008.03	0.65 (+0.15)	0.06	0.12	−0.03	0.05
16	2008.04-2011.07	0.78 (+0.11)	0.03	0.05	−0.02	0.02
17	2011.08-2018.02	0.83 (+0.20)	0.01	−0.02	−0.05	−0.02
18	2018.03-2021.03	1.09 (+0.09)	−0.02	−0.07	−0.09	−0.06

Note: The GCB estimate represents the multi-model mean of the three bookkeeping models. The AGMT value reported in the third column for each peak is computed as the sum of the baseline anomaly and the corresponding fluctuation.

Table 1 presents E_{LUC} averages over each of the 1950–2021 peaks alongside the AGMT anomalies

for the same periods. Notably, the interval spanning 1982.6–1989.3, which includes the 10th and 11th peaks, represents a transition period during which AGMT hovers around 0.5 °C. Prior to the 10th peak (1982.6), the temperature anomalies oscillate around lower values, while after the 12th peak (1989.4) the AGMT exceeds 0.5 °C. By combining the E_{LUC} and AGMT data reported in Table 1, we reconstruct the evolving statistical relationship between carbon emissions and temperature anomalies, effectively providing the detailed instantiation of the E_{LUC}–AGMT relationship shown in Fig. 5. Fig. 8 displays the E_{LUC}–AGMT scatter for the 10th through 18th peaks (1982.6–2021.3), with linear regressions fitted to each bookkeeping-model estimate as well as the GCB multi-model mean.

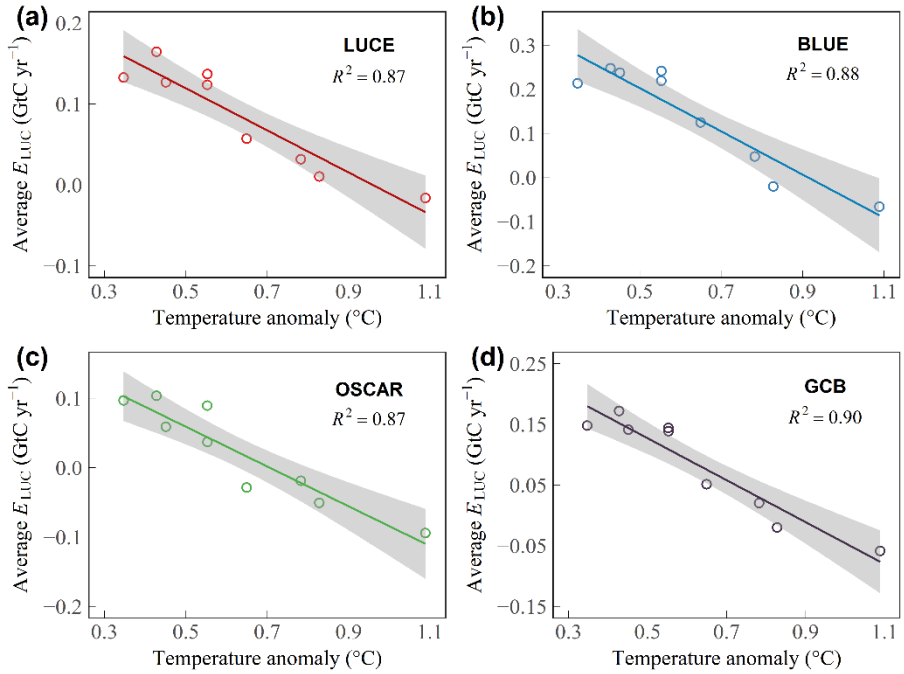

Fig. 8 Relationship between China's land-use change-induced carbon emissions (E_{LUC}) and the global annual mean temperature anomaly (AGMT) for the 10th through 18th peaks (1982.6–2021.3). Panels (**a**)–(**c**) correspond to LUCE, BLUE, and OSCAR bookkeeping models, respectively, and panel (**d**) shows the GCB ensemble average. Solid lines depict fitted linear relationships, with shaded areas representing 95% confidence intervals

4.2 Classification of attributable complex systems

In Section 3.2, we examined the essential dynamics of LUC, operating under the assumption that they can be captured through low-dimensional representations. While LUC is clearly a complex system, it is useful to further classify its nature within the framework of attributable complex systems. Using response theory for nonequilibrium systems, observables Y_k (k=1,…,S) can be decomposed as

$$Y_k = \sum_{p=1}^{M} x_k^p \qquad (k=1,\ldots,S), \tag{4}$$

where each x_k^p represents one of M characteristic response patterns (or fingerprints), each associated with a distinct forcing. Although interactions among these fingerprints may introduce higher-order terms, such contributions can be absorbed or eliminated through linear regression (Lucarini and Chekroun 2024). This decomposition underpins the classification of attributable complex systems: if

there exists an index i such that

$$|Y_i|/\sum_k^s |Y_k| \cong O(1), \tag{5}$$

then the system is identified as an attributable complex system with a main cause (ACSMC). Otherwise, it is categorized as an attributable complex system without a main cause (ACSN-C).

Given the well-established role of anthropogenic (notably CO_2) emissions as the dominant driver of global warming, and acknowledging the central position of LUC within the carbon budget, we view Eq. (5) as satisfied for the LUC subsystem. Deforestation, urbanization, and agriculture across different regions collectively provide the dominant fingerprint of this system. The successful single-peak segmentation of E_{LUC} versus time (Fig. 3) confirms the existence of this fingerprint and supports the interpretation of LUC as an ACSMC. We conjecture that this classification framework could have broad applicability beyond climate science, for instance in quantitative social sciences. ACSMCs satisfy Whitney's embedding theorem (Whitney 1936), so their evolution can be reconstructed through low-dimensional embeddings. By contrast, ACSN-C systems, lacking a clear dominant fingerprint, remain inherently difficult to forecast.

4.3 Summary

Land-use change-induced carbon emissions (E_{LUC})—defined as the net of emissions and removals—have contributed roughly one-third of global anthropogenic carbon emissions since the onset of industrialization. The complex temporal evolution of E_{LUC} observed both globally and in China underscores its significance for understanding climate change and highlights land-use change as a key lever for climate mitigation.

We interpret LUC as an attributable complex system with a main cause (ACSMC): the combined effects of deforestation, urbanization, and agriculture across multiple regions act as the optimal fingerprint for the system. The segmentation of E_{LUC} evolution shown in Fig. 3 reveals three phases: an increasing phase before 1913, a Gaussian-peak phase between 1913 and 1992, and a decreasing phase after 1992.

During this third phase, we identify a negative correlation between E_{LUC} and AGMT (for AGMT > 0.4 °C), indicative of E_{LUC} adaptation at higher temperatures. Concurrently, the temperature sensitivity parameter $\Delta E_{\mathrm{LUC}}(T_0)$ increases for $T_0 > 0.5$ °C, reflecting an accelerating rate of E_{LUC} decline with warming. Table 1 further pinpoints the transition period between the 10th and 11th peaks (1982.6–1989.3), when AGMT crosses 0.5 °C, suggesting that E_{LUC} adaptation began around April 1989. Through this adaptation, the initial E_{LUC} amplification induced by warming can gradually subside or even approach pre-warming levels over intermediate to long timescales, thereby attenuating the positive carbon–climate feedback.

References

Cleveland WS (1979) Robust locally weighted regression and smoothing scatterplots. J Am Stat Assoc 74:829-836. https://doi.org/10.1080/01621459.1979.10481038

Foley JA, Prentice IC, Ramankutty N, Levis S, Pollard D, Sitch S, Haxeltine A (1996) An integrated biosphere model of land surface processes, terrestrial carbon balance, and vegetation dynamics. Glob Biogeochem Cycle 10:603–628. https://doi.org/10.1029/96gb02692

Friedlingstein P et al (2022) Global Carbon Budget 2022. Earth Syst Sci Data 14: 4811–4900. https://doi.org/10.5194/essd-14-4811-2022

Friedlingstein P et al (2025) Global Carbon Budget 2025. Earth Syst. Sci. Data Discuss. [preprint], https://doi.org/10.5194/essd-2025-659

Gasser T, Crepin L, Quilcaille Y, Houghton RA, Ciais P, Obersteiner M (2020) Historical CO_2 emissions from land use and land cover change and their uncertainty. Biogeosciences 17:4075–4101. https://doi.org/10.5194/bg-17-4075-2020

Grassi G et al (2023) Harmonising the land-use flux estimates of global models and national inventories for 2000–2020. Earth Syst Sci Data 15:1093–1114. https://doi.org/10.5194/essd-15-1093-2023

Hansis E, Davis SJ, Pongratz J (2015) Relevance of methodological choices for accounting of land use change carbon fluxes. Glob Biogeochem Cycle 29:1230–1246. https://doi.org/10.1002/2014gb004997

Holland JH (1992) Adaptation in natural and artificial systems: an introductory analysis with applications to biology, control, and artificial intelligence. MIT Press, Cambridge. https://doi.org/10.7551/mitpress/1090.001.0001

Lenssen N, Schmidt GA, Hendrickson M, Jacobs P, Menne M, Ruedy R (2024) A NASA GISTEMPv4 observational uncertainty ensemble. JGR Atmospheres 129: e2023JD040179. https://doi.org/10.1029/2023jd040179

Lucarini V, Chekroun MD (2024) Detecting and attributing change in climate and complex aystems: Foundations, Green's functions, and nonlinear fingerprints. Phys Rev Lett 133: 244201. https://doi.org/10.1103/physrevlett.133.244201

Qin Z, Zhu Y, Canadell JG, Chen M, Li T, Mishra U, Yuan W (2024) Global spatially explicit carbon emissions from land-use change over the past six decades (1961–2020). One Earth 7:835–847. https://doi.org/10.1016/j.oneear.2024.04.002

Takens F (1981) Detecting strange attractors in turbulence. In: Rand D, Young LS (eds) Dynamical Systems and Turbulence, Warwick 1980. Lecture notes in mathematics, vol 898. Springer, Berlin Heidelberg, pp 366–381. https://doi.org/10.1007/BFb0091924

Whitney H (1936) Differentiable Manifolds. The Annals of Mathematics 37:645–680. https://doi.org/10.2307/1968482

Wu T, Gao X, An F, Sun X, An H, Su Z, Gupta S, Gao J, Kurths J (2024) Predicting multiple observations in complex systems through low-dimensional embeddings. Nat Commun 15:2242. https://doi.org/10.1038/s41467-024-46598-w

Zhu Y, Xia X, Canadell JG, Piao S, Lu X, Mishra U, Wang X, Yuan W, Qin Z (2025) China's carbon sinks from land-use change underestimated. Nat Clim Chang 15:428–435. https://doi.org/10.1038/s41558-025-02296-z

Statements and Declarations

Funding

This research did not receive any specific grant from funding agencies in the public, commercial, or not-for-profit sectors.

Competing Interests

The authors have no relevant financial or non-financial interests to disclose.

Author Contributions

Jun Lv: data collection, software, visualization, formal analysis, validation and critical feedback on the manuscript. Liaofu Luo: study design, methodology, and writing–original draft. All authors: writing–review and editing. All authors have read and agreed to the published version of the manuscript.

Data Availability

Two data sets used in this study are available at the following links: Carbon emissions data are publicly available at the link: https://doi.org/10.18160/gcp-2025; Global annual and monthly mean surface temperature anomalies data are publicly available at the link: https://data.giss.nasa.gov/gistemp/.